ACS Chemical Neuroscience

Research Article

pubs.acs.org/chemneuro

Investigation of a Calcium-Responsive Contrast Agent in Cellular Model Systems: Feasibility for Use as a Smart Molecular Probe in Functional MRI

Goran Angelovski,*[,†] Sven Gottschalk,[‡] Milena Milošević,[∥] Jörn Engelmann,[‡] Gisela E. Hagberg,[‡,⊥] Pascal Kadjane,[§] Pavle Andjus,[∥] and Nikos K. Logothetis[§,#]

[†]MR Neuroimaging Agents, [‡]High-Field Magnetic Resonance, [§]Physiology of Cognitive Processes, Max Planck Institute for Biological Cybernetics, 72076 Tübingen, Germany

[∥]Institute for Physiology and Biochemistry, Faculty of Biology, University of Belgrade, Beograd 11000, Serbia

[⊥]Biomedical Magnetic Resonance, Department of Radiology, Tübingen University Hospital, 72076 Tübingen, Germany

[#]Division of Imaging Science and Biomedical Engineering, University of Manchester, Manchester M13 9PL, United Kingdom

ABSTRACT: Responsive or smart contrast agents (SCAs) represent a promising direction for development of novel functional MRI (fMRI) methods for the eventual noninvasive assessment of brain function. In particular, SCAs that respond to Ca^{2+} may allow tracking neuronal activity independent of brain vasculature, thus avoiding the characteristic limitations of current fMRI techniques. Here we report an in vitro proof-of-principle study with a Ca^{2+}-sensitive, Gd^{3+}-based SCA in an attempt to validate its potential use as a functional in vivo marker. First, we quantified its relaxometric response in a complex 3D cell culture model. Subsequently, we examined potential changes in the functionality of primary glial cells following administration of this SCA. Monitoring intracellular Ca^{2+} showed that, despite a reduction in the Ca^{2+} level, transport of Ca^{2+} through the plasma membrane remained unaffected, while stimulation with ATP induced Ca^{2+}-transients suggested normal cellular signaling in the presence of low millimolar SCA concentrations. SCAs merely lowered the intracellular Ca^{2+} level. Finally, we estimated the longitudinal relaxation times (T_1) for an idealized in vivo fMRI experiment with SCA, for extracellular Ca^{2+} concentration level changes expected during intense neuronal activity which takes place upon repetitive stimulation. The values we obtained indicate changes in T_1 of around 1−6%, sufficient to be robustly detectable using modern MRI methods in high field scanners. Our results encourage further attempts to develop even more potent SCAs and appropriate fMRI protocols. This would result in novel methods that allow monitoring of essential physiological processes at the cellular and molecular level.

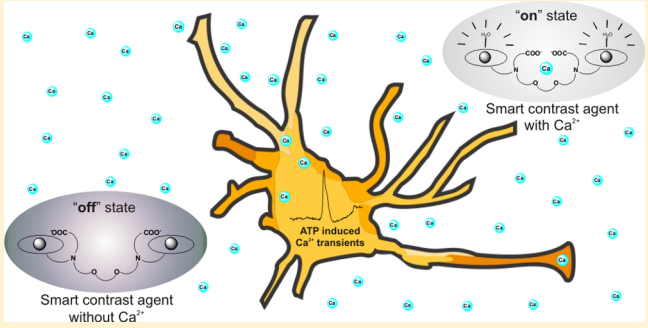

KEYWORDS: *Calcium, functional magnetic resonance imaging, responsive/smart contrast agents*

The crucial role of calcium in neural signaling processes has been extensively investigated over the past few decades. Numerous methodological approaches were reported, especially those attempting to measure intracellular calcium, aiming to understand basic physiological processes and to enable reliable monitoring of brain function. On the other hand, investigating the extracellular calcium signaling has been mostly overlooked, despite its occasional large reductions in the intercellular space.[1] Practical issues were probably the main reason for currently better knowledge on intracellular calcium signaling. Namely, the isolated cells are conveniently followed in a dish rather than in large volumes with numerous cells by majority of conventional techniques.

Either way, different approaches have been taken for the development of efficient calcium indicators; thus far, the vast majority of information was obtained using fluorescent indicators, either synthetic or genetically encoded.[2,3] However, the limitations of fluorescence-based methods related to their limited depth of penetration into tissues argues for the development of techniques to circumvent such problems. In particular, imaging techniques based on magnetic resonance are of interest due to their unlimited depth penetration. Pioneering attempts to establish NMR as the method of choice for this employed ^{19}F-labeled 1,2-bis(o-aminophenoxy)ethane-*N*,*N*,*N*′,*N*′-tetraacetic acid (BAPTA) molecules.[4] The importance of magnetic resonance imaging (MRI) for monitoring neural function dramatically increased with the description of functional MRI (fMRI) based on blood oxygen level-dependent (BOLD) contrast,[5] making this method the primary choice in modern neuroimaging. Nevertheless, BOLD fMRI has inherent limitations.[6] It measures a surrogate signal resulting from the neurovacular coupling where the obtained spatiotemporal

Received: November 7, 2013
Revised: March 26, 2014
Published: April 8, 2014

information is heavily dependent on the brain's vasculature and its specific physiological responses. Therefore, a more direct measurement of neural signaling, for example, by following alterations in calcium fluctuations, remains of great interest.

The first responsive or "smart" contrast agent (SCA) suitable for MRI was based on the same calcium chelator (BAPTA) as its predecessor for fluorescence imaging or ^{19}F NMR spectrosopy.[7] In the past decade, there have been a number of attempts to prepare calcium-sensitive MRI contrast agents, using either paramagnetic T_1,[8] superparamagnetic T_2,[9] or PARACEST agents.[10] However, to the best of our knowledge, there are no reports of in vivo fMRI with any of these agents so far, and it is currently not clear whether they will be able to generate sufficient MR-signal changes to be observable in an in vivo MRI experiment. On the other hand, were the MR responses of the SCAs to be sufficiently robust, it is not known whether their presence might influence standard cellular physiological processes, thus preventing normal neural signaling and consequently calcium fluctuations. Finally, a number of technological issues such as appropriate animal preparation, MRI protocols, and data analysis are crucial to accomplish successful fMRI experiments using smart MR contrast agents.

In the present work, we performed an in vitro proof-of-principle study and investigated SCA responses in a complex cellular system that can potentially predict in vivo SCA behavior. Specifically, we measured the amplitude of T_1 changes as a function of Ca^{2+} concentration in a 3D cell culture model (fibroblasts embedded in an extracellular matrix gel) that, at least to some extent, mimics the environment of a biological tissue. Furthermore, we monitored changes in intracellular Ca^{2+} and ATP-induced Ca^{2+}-transients upon the addition of SCA to primary glial cells (conventional 2D cultures of astrocytes) by means of laser scanning confocal microscopy using Ca^{2+}-sensitive fluorescent probes. Finally, based on the data obtained from these model studies, we calculated the expected longitudinal relaxation times for an idealized in vivo fMRI experiment with SCA, and investigated whether extracellular calcium fluctuations from 1.2 to 0.8 mM, present during intense neuronal activity and triggered by robust stimuli,[11−13] are capable of yielding detectable T_1 changes by means of MRI.

RESULTS

All studies described in this work were performed using the dinuclear gadolinium complex Gd_2L with an EGTA-derived (ethylene glycol-bis(β-aminoethyl ether)-*N*,*N*,*N*′,*N*′-tetraacetic acid) moiety which connects two macrocyclic, DO3A-type chelators and serves as a selective chelator of Ca^{2+} (Figure 1a). A pair of such SCAs was recently reported by our group, in which Gd_2L, the analogue possessing propyl linkers, exhibited a higher longitudinal relaxivity (r_1) response in the presence of Ca^{2+}.[14] In HEPES buffer, the maximal observed increase in r_1 was 82%, whereas the maximal increase in the brain extracellular model (a medium that resembles brain extracellular fluid) was 52%, presumably due to the presence of anions that form ternary complexes with DO3A-type systems.[15]

Relaxometric Titrations. The relaxometric titrations were performed for Gd_2L at 37 °C in the same cell culture medium (CCM) that was used for the 3D cell culture model (NIH-3T3 fibroblasts embedded in Matrigel; see below), in order to fully characterize the behavior of Gd_2L under the conditions studied. We used the same conditions in terms of specific medium combinations and appropriate NMR instrumentation (7 T), to allow direct comparison of the results. For seven independent

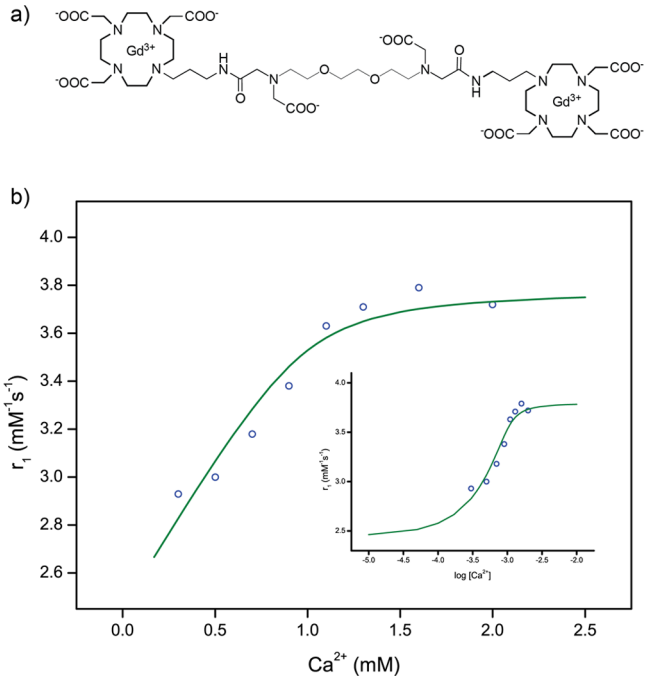

Figure 1. (a) Chemical structure of the investigated smart contrast agent Gd_2L. (b) Representative relaxometric Ca^{2+} titration in CCM at 7 T and 37 °C, [Gd_2L] = 1.0 mM. The line represents the result for fitting as described in the Methods section, assuming a single binding site, with K_d = 47.3 μM, $r_{1,f}$ = 2.45 mM^{-1} s^{-1} and $r_{1,b}$ = 3.79 mM^{-1} s^{-1}. The inset shows same data on a logarithmic scale for the *x*-axis.

titrations, Gd_2L (1.0 or 1.8 mM) was dissolved in CCM containing different Ca^{2+} concentrations, T_1 values of the solutions were determined for each Ca^{2+} concentration, and respective r_1 values were calculated (a single representative titration is shown in Figure 1b). Curve fitting was performed for each individual experiment according to eq 2 (Methods section) and resulted in a mean conditional dissociation constant K_d = 45.4 ± 28.0 μM (mean ± standard deviation (SD), n = 7), which fully corresponds to the value previously obtained for the same SCA in a slightly different medium.[14] The $r_{1,f}$ relaxivity of the free SCA (in the absence of Ca^{2+}) was 2.42 ± 0.19 mM^{-1} s^{-1} (mean ± SD, n = 7), whereas the $r_{1,b}$ relaxivity value of the SCA fully bound to Ca^{2+} was 3.64 ± 0.13 mM^{-1} s^{-1} (mean ± SD, n = 7). The values of K_d and $r_{1,f/b}$ obtained in this way were used to calculate the theoretically expected T_1 values in all subsequent experiments (see below).

It should be noted that two different approaches were used for sample preparation (see Methods section). In both cases, a drop in r_1 values of ∼10% was observed for samples at higher Ca^{2+} concentrations (3−4 equiv) that were measured >2 h after preparing the solutions. Despite using a buffered CCM (20 mM HEPES), a slight increase in the pH of these samples (up to 1 pH unit) was associated with this phenomenon. Thus, only values up to 2 equiv of Ca^{2+} were used for fitting the curves.

NMR Studies of SCA within a Cellular Environment. Despite the development of a number of SCAs reported in the past decade, translation to in vivo applications is still very challenging. For instance, in many cases, it is still not clear whether the r_1 changes observed in a buffered solution or more complex media are actually sufficient for in vivo detection. One of the great obstacles is the nature of the soft tissue, consisting of cells and the extracellular space (ECS). In brain, ECS accounts for approximately 20% of the volume;[16] therefore,

dx.doi.org/10.1021/cn500049n | ACS Chem. Neurosci. 2014, 5, 360−369

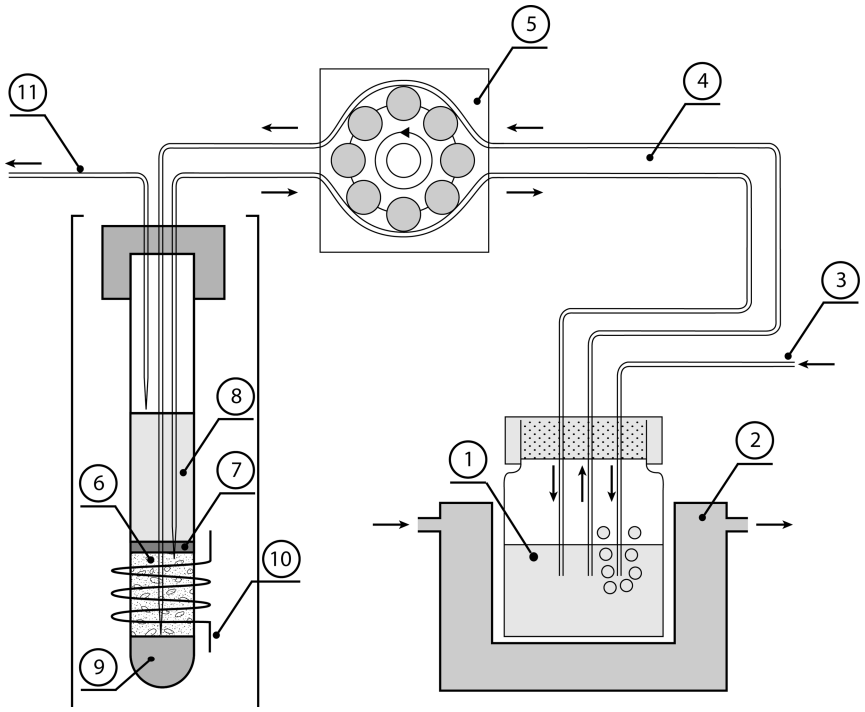

Figure 2. Setup used for T_1 determination in the model system where 3D cells-Matrigel culture is perfused with CCM containing SCA. The setup consisted of the following components: (1) reservoir of the SCA solution in CCM; (2) thermostated water bath; (3) Carbogen bubbling line; (4) the lines for pumping SCA solution to and from the NMR tube; (5) peristaltic pump; (6) cells-Matrigel inside the NMR tube; (7) glass frit; (8) SCA solution in CCM above the glass frit and cells-Matrigel; (9) Teflon plug; (10) NMR spectrometer coil; (11) the line to the backup peristaltic pump, also leading back to 1 (not shown for more clarity).

signals arising from extracellular SCA are weak due to detection only from the partial, active volume. On the other hand, if an intracellular SCA is used, the "attenuation" of the MR signal due to this effect would not be very prominent, as SCA would be present in ∼80% volume occupied by cells. However, it should be noted that very high amounts of SCA are needed for delivery into cells in order to achieve robust MR signal changes. This requires considerable efforts in modifying the SCA structure to improve cell internalization.

This very fact underlies the efforts required to achieve the best possible signal-to-noise ratio and specificity for each molecule developed (e.g., maximal r_1 changes for T_1 agents). Consequently, respective optimizations can best be carried out in vitro. To simulate tissue conditions, we designed a model system that mimics living tissues with regard to density, partially occupied (extracellular) volume, and flow conditions. Growing fibroblast cells (NIH-3T3) as 3D cultures embedded in an extracellular basement membrane matrix gel (Matrigel)[17] were used to simulate tissues populated with cells. Matrigel was used to ensure cell adhesion, viability, and growth performance, and to minimize perturbations which can be generated from the circulating CCM. The cells were perfused with a CCM, which was thermostated outside the NMR spectrometer and through which Carbogen gas (95% O_2/5% CO_2) was bubbled throughout the experiment to ensure sufficient oxygen supply to the cells. During the course of the experiment, which usually lasted for 3−4 h, the CCM supplied sufficient nutrients for the cells to survive. The perfusion also simulated in vivo flow conditions, where cells were supplied with fresh nutrients and oxygen while at the same time metabolic waste products were removed. Cells embedded in Matrigel (cells-Matrigel) were placed in an NMR tube of 5 mm diameter covering the complete sensitive volume of the coil. A porous glass frit was used as a cover, to keep the membrane threads in place, while oxygenized CCM was pumped into the NMR tube (Figure 2). The Ca^{2+} concentration in the CCM was adjusted to 1.2 mM, a value estimated to represent the ECS in the resting state of the brain.[13]

At the beginning of the experiments, a ^{31}P NMR spectrum was recorded in order to ascertain cell viability. The spectra exhibited a normal energy charge of the cells with α-, β- and γ-nucleoside triphosphate (NTP) signals being present,[18] thus indicating a sufficient amount of viable cells in the cells-Matrigel (Figure 3, lower spectrum). A defined amount of the solid SCA was dissolved in CCM to achieve 1.2 mM SCA concentration, which is equimolar to Ca^{2+} (see above). Upon concentration equilibration for ∼15 min, the T_1 value of the SCA solution was determined and compared with the theoretical T_1 (Table 1), calculated from the fitted curve (Figure 1b). As expected for the tissue model, longer T_1 values were experimentally obtained, depending on the exact density of the cells-Matrigel portion (estimated for every experiment, ∼35−50% of the total volume). Namely, the presence of the cells and in particular exchange of intracellular and extracellular water protons modulate the overall T_1 value in the sensitive volume of the coil. This demonstrates the occurrence of an "active volume" portion, which reduces the actual effect of SCA on T_1.

Next, we manipulated the extracellular Ca^{2+} concentration ($[Ca^{2+}]_o$) and determined ΔT_1 by performing the same inversion recovery experiments as in the relaxometric titrations (see above). A defined amount of EDTA from a stock solution (0.5 M) was added to the CCM to achieve 0.8 mM Ca^{2+} concentration, a reduction in Ca^{2+} that is also reached in vivo

dx.doi.org/10.1021/cn500049n | ACS Chem. Neurosci. 2014, 5, 360−369

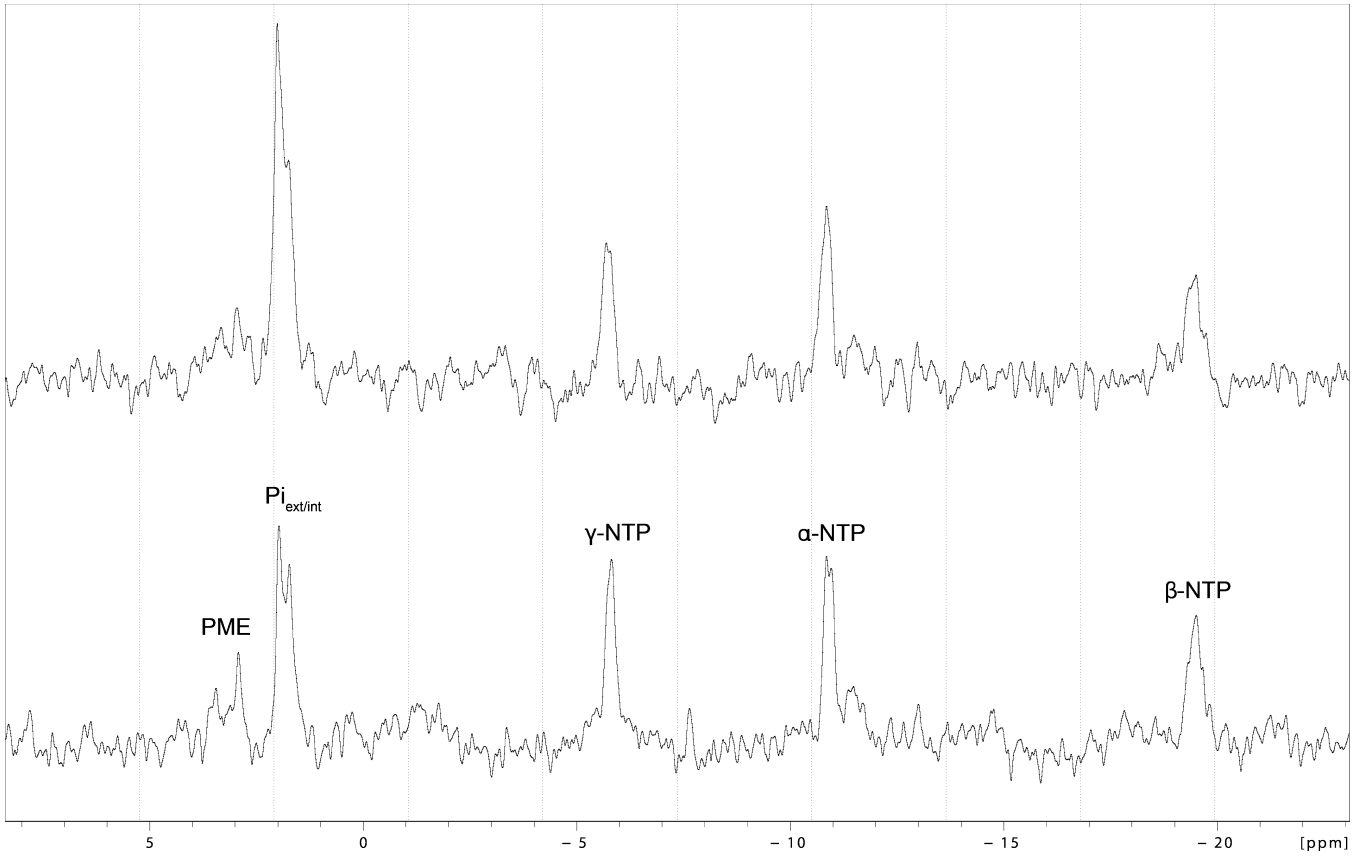

Figure 3. Cell viability in the 3D cell culture model. Representative ^{31}P NMR spectra of cells embedded in Matrigel at the beginning (bottom) and end (top) of the experiments (approximately after 3.5 h) at 37 °C in CCM. Abbreviations: *α*-, *β*-, or *γ*-NTP, nucleoside triphosphates; $Pi_{ext/int}$, extra- and intracellular inorganic phosphate; PME, phosphomonoesters.

Table 1. T_1 Values Obtained from Three Different Experiments with Cells Embedded in Matrigel in the Presence of Gd_2L (1.2 mM), and Comparison with Theoretically Calculated Values (without cells in Matrigel)

	T_1 (ms)			
simulated condition	exp no. 1	exp no. 2	exp no. 3	theor T_1[d]
"resting state" (1.2 mM Ca^{2+})[a]	141.6 ± 0.6[e]	143.6 ± 0.1[e]	130.8 ± 0.1[e]	117.3
"activated state" (0.8 mM Ca^{2+})[b]	145.7 ± 0.2[e,**,##]	146.4 ± 0.1[e,***,##]	133.8 ± 0.3[e,***,##]	126.3
ΔT_1	4.1 (2.9%)	2.8 (2.0%)	3.0 (2.3%)	9.0
"resting state" (1.2 mM Ca^{2+})[c]	142.0 ± 0.6[e]	145.0 ± 0.3[e]	132.2 ± 0.2[e]	117.3

[a]$[Ca^{2+}]$ was adjusted in the CCM before the experiment. [b]Calculated volume of an EDTA stock solution was added to adjust CCM to the desired $[Ca^{2+}]$. [c]Calculated volume of a Ca^{2+} stock solution was added to the CCM to return the $[Ca^{2+}]$ to 1.2 mM. [d]T_1 value calculated from the fitted r_1 values (Figure 1b), assuming absence of cells in Matrigel (estimated extracellular fraction, EF = 1); see Table 2. [e]Values represent mean ± SEM (n = 3 consecutive measurements of T_1 at each condition) except for ΔT_1. $^{**}p < 0.01$; $^{***}p < 0.001$ statistical significant difference vs initial resting state (1.2 mM Ca^{2+}); $^{\#\#}p < 0.01$ statistical significant difference vs resting state (1.2 mM Ca^{2+}) after recovery (ANOVA, Tukey's multiple comparison post-test).

during intense brain stimulation.[11,13] On CCM equilibration, a set of T_1 values was recorded, revealing a statistical significant mean increase of 3.3 ± 0.4 ms (2.4 ± 0.3%, n = 3 independent repetitions, $p < 0.01$, unpaired Student's t-test) in T_1 (decrease in r_1) when compared to the initial "resting state" conditions of 1.2 mM Ca^{2+} (Table 1).

The reversibility of the SCA response was tested by adding Ca^{2+} to the CCM, thus returning to the initial 1.2 mM concentration (now excluding the bound Ca^{2+} portion in the Ca-EDTA complex). Immediately after CCM equilibration, the T_1 values approached those recorded at the beginning of the experiment at the "resting state" Ca^{2+} concentration (1.2 mM), though still slightly higher (Table 1), resulting in a T_1 difference of 1.0 ± 0.4 ms compared to the "resting state" T_1 at the beginning of the experiment. However, the ΔT_1 of the "activated state" was still significantly higher than the difference between the two "resting state" T_1 values (3.3 ± 0.4 ms vs 1.0 ± 0.4 ms, $p < 0.01$).

At the end of each experiment, another ^{31}P NMR spectrum was recorded (Figure 3, upper spectrum). The resonances of *α*-, *β*-, and *γ*-NTP groups were still clearly detectable, albeit at lower signal intensities concomitant with an increase of the inorganic phosphate signal compared to the ^{31}P NMR spectrum at the beginning of the experiment. This indicates a loss of living cells during the course of NMR measurements.

Control experiments were performed using Dotarem (GdDOTA) in the presence of Polybead microspheres or cells-Matrigel composites. The microspheres are based on

dx.doi.org/10.1021/cn500049n | ACS Chem. Neurosci. 2014, 5, 360−369

polystyrene and in analogy to the cells-Matrigel model also occupied ~50% of the total volume, thus simulating living tissue in terms of the active volume that can be affected by the contrast agent. However, the experimental T_1 values obtained in the presence of Polybead microspheres fully corresponded to theoretical T_1 values because the "effective" volume equaled the ECS volume. In this case, no water is present inside the microspheres, and hence, there is no apparent "dilution" of SCA concentration.

Furthermore, studies with Dotarem and the cells-Matrigel composites produced the same results as in the case of SCA; that is, the experimental T_1 was always longer than the T_1 obtained without the cells-Matrigel composites (data not shown). Finally, performing the same "resting–activated–resting states" paradigm as was used with SCA in the cells-Matrigel model by adding EDTA and Ca^{2+} to Dotarem dissolved in CCM only, did not result in any T_1 changes (data not shown).

Monitoring Intracellular Ca^{2+} Changes. Astrocytes are one of the most abundant and functionally significant cells in the brain. We selected them for use as a conventional in vitro cell culture model for testing possible biological effects of SCA. These tests were done by monitoring intracellular Ca^{2+}-concentration, cell signaling, and viability in primary astrocytes. Ca^{2+}-signaling in nonexcitable as well as in excitable cells is based on the maintenance of a low concentration of cytosolic free Ca^{2+} (<200 nM) as compared to the extracellular compartment (1–2 mM) and intracellular Ca^{2+}-stores (0.1–1 mM).[19,20] Due to this distribution, a gradient is formed across the plasma and the subcellular membranes (the latter delimiting endoplasmatic reticulum (ER), mitochondria, and lysosomes).

First, we determined whether the binding capacity of Gd_2L may also affect intracellular Ca^{2+}-concentrations. We used laser scanning confocal microscopy imaging and the Ca^{2+}-sensitive fluorescent probe Fluo-4. Gd_2L was applied extracellularly in three different concentrations, equimolar to $[Ca^{2+}]_o$ (1.2 mM), 50% lower, or 50% higher (0.6 or 1.8 mM, respectively). A decrease in intracellular Ca^{2+} was observed in response to all three concentrations of SCA, with a similar time course (Figure 4). All concentrations tested induced an exponential decline in cytosolic free Ca^{2+}, stabilizing at the diminished level of 64–67% about 5 min after the addition of the probe (Figure 4, inset Table). There were no significant differences in relative fluorescence intensity at the 5 min time point regardless of the SCA concentration.

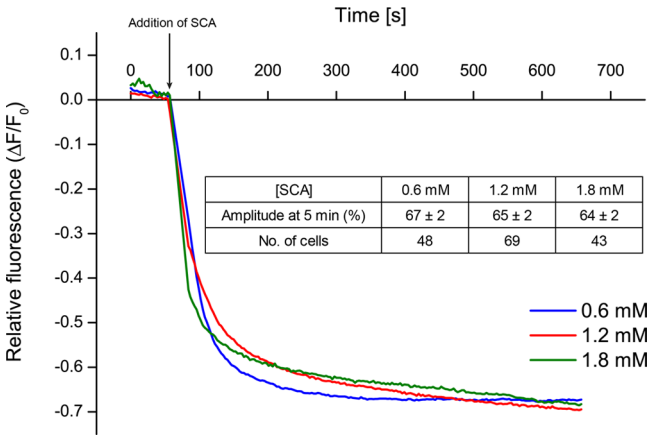

[SCA]	0.6 mM	1.2 mM	1.8 mM
Amplitude at 5 min (%)	67 ± 2	65 ± 2	64 ± 2
No. of cells	48	69	43

Figure 4. SCA lowers the intracellular Ca^{2+} concentration in cultured astrocytes. Relative decline of $[Ca^{2+}]_i$ following the application of three concentrations of SCA (indicated by colored lines). Inset: Table presenting relative decrease of $[Ca^{2+}]_i$ (mean ± standard error) 5 min after SCA application, with the number of counted astrocytes given.

The major source of Ca^{2+} in astrocytes resides within the ER, which is endowed with inositol 1,4,5-trisphosphate ($InsP_3$) and ryanodine receptors. When activated, these receptors mediate the release of Ca^{2+} into the cytosol.[21] Refilling of the ER stores is attributed to the sarco-endoplasmic reticulum Ca^{2+}-ATPase (SERCA), while the depletion of intracellular stores additionally draws Ca^{2+} from the extracellular space via store-operated calcium entry (SOCE).[22] An alternative, albeit less-studied pathway for Ca^{2+} entry is associated with the plasma membrane Na^+-Ca^{2+} exchanger (NCX).[23] These pathways were pharmacologically tested here in order to understand the mechanisms underlying cytosolic Ca^{2+} loss in response to SCA.

To estimate the contribution of the SOCE pathway, two types of experiments were conducted. In the first set of experiments, calcium was omitted from the external solution, while in the second set SOCE was blocked by the use of specific pharmacological agents, a combination of trivalent cations (La^{3+} and Gd^{3+}) that block SOCE fully in the low micromolar range,[24] and 2-amino-ethoxydiphenylborane (2-APB), a membrane-permeable inhibitor of $InsP_3$ receptor function, recently recognized as a direct inhibitor of SOCE.[25] The decrease of cytosolic Ca^{2+} concentration in response to 1.2 mM SCA was then measured and compared to the values already obtained in the standard external solution. The SCA-induced decrease of cytosolic Ca^{2+} was reduced to 39 ± 1% (n = 48) by omitting Ca^{2+} from the external solution, and to 43 ± 2% (n = 11) under pharmacological blockade of the SOCE pathway (Figure 5). These values are significantly different from the data obtained in standard external solution, but not from each other. Overall, as compared to SCA-induced decreased cytosolic Ca^{2+} in standard external solution, these data suggest that ~20–25% of cytosolic Ca^{2+} has been taken up through the SOCE pathway.

The contribution of SERCA was estimated in a subset of experiments where thapsigargin, a potent inhibitor of SERCA,[26] was used in addition to SOCE pharmacological blockers (defined above). The SCA-induced loss of cytosolic Ca^{2+} under these conditions was decreased to 30 ± 1% (n = 40) (Figure 5). Compared with the value obtained under conditions of blocked SOCE, this points to ~10–15% of Ca^{2+} decay as being attributable to the activity of SERCA.

The involvement of NCX in SCA-induced decay of cytosolic Ca^{2+} was estimated in the next set of experiments using the NCX-specific blocker, benzamil hydrochloride.[27,28] When applied alone, this blocker revealed an SCA-induced Ca^{2+} decay of 41 ± 2% (n = 41), while in combination with SOCE and SERCA blockers the decrease in the presence of SCA was reduced to 11 ± 1% (n = 24) (Figure 5). When each set of data was compared to the values obtained without benzamil hydrochloride (SCA in standard external solution, or with SOCE and SERCA blocked), the implication is that ~20% of Ca^{2+} decrease could be attributed to the activity of NCX.

Any potential acute toxicity of SCA toward astrocytes was assessed by the MTT viability assay. Astrocytes were treated with three concentrations of SCA (0.6, 1.2, and 1.8 mM) for 4 h, which corresponds to the duration and the local SCA concentrations in the projected in vivo experiment.[29] This MRI probe was shown not to affect cell viability at any of the concentrations used (Figure 6a).

dx.doi.org/10.1021/cn500049n | ACS Chem. Neurosci. 2014, 5, 360–369

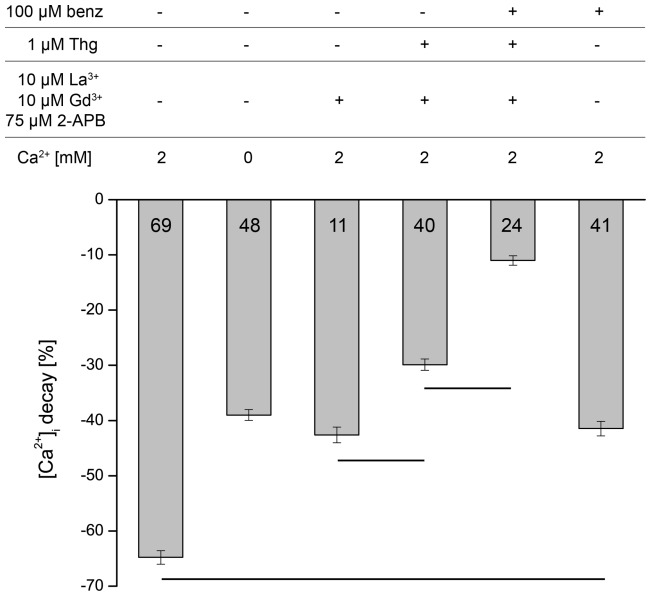

Figure 5. Pharmacological identification of pathways for $[Ca^{2+}]_i$ loss. Relative decline of $[Ca^{2+}]_i$ measured 5 min after application of 1.2 mM SCA in astrocytes pretreated with specific blockers (La^{3+}, lanthanum chloride; Gd^{3+}, gadolinium chloride, 2-APB, 2-aminoethoxydiphenyl borate; Thg, thapsigargin; benz, benzamil hydrochloride) in the presence (2 mM) or absence of extracellular calcium. Numbers of counted/analyzed astrocytes are presented at the bar bases. Statistically significant differences ($p < 0.001$, ANOVA with Dunn's post hoc multiple pairwise test) between treatment groups are indicated by horizontal lines connecting respective vertical bars.

Finally, the physiological conditions and the calcium signaling capacity of astrocytes was estimated by their response to 1 mM ATP in the presence of SCA. ATP was used as a physiological stimulus and should lead to an increase in intracellular Ca^{2+} as a consequence of a Ca^{2+} transient, expected to arise from intracellular stores as well as the extracellular space through the purinergic ion channels.[30,31] First, the cells were treated with 1.2 mM SCA for 45 min, and after equilibration the responses to ATP were recorded, in the presence of SCA. Astrocytes responded with a robust biphasic transient increase in the intracellular concentration of calcium, $[Ca^{2+}]_i$ (Figure 6b).

Simulations of T_1 in Vivo. Because the NMR and the intracellular Ca^{2+} studies described above encourage the use of SCA in vivo, we performed a simulation of T_1 values in a hypothetical idealized experiment. We calculated the expected T_1 at two different Ca^{2+} concentrations, 1.2 mM (assumed to represent the "baseline" state) and 0.8 mM (assumed to represent the "active" state), using the values for K_d and $r_{1,f/b}$ described above. Furthermore, predictions were made for three different conditions: in the absence of cells (in vitro experiments in CCM; see above), in the presence of cells (in vitro experiments in Matrigel; see above), and in vivo (hypothetical experiments). The estimated T_1 values were obtained using eq 3 (see Methods section), which accounts for the different extracellular volume fractions and diamagnetic contributions of water molecules inside the cells. Namely, the local concentration of SCA in a given volume proportionally decreases with the increase in the cellular fraction along with the $T_{1,d}$ shortening due to the higher amount of water inside the cells that leads to the apparent reduction of SCA concentration. On the other hand, the initial, "nondiluted"

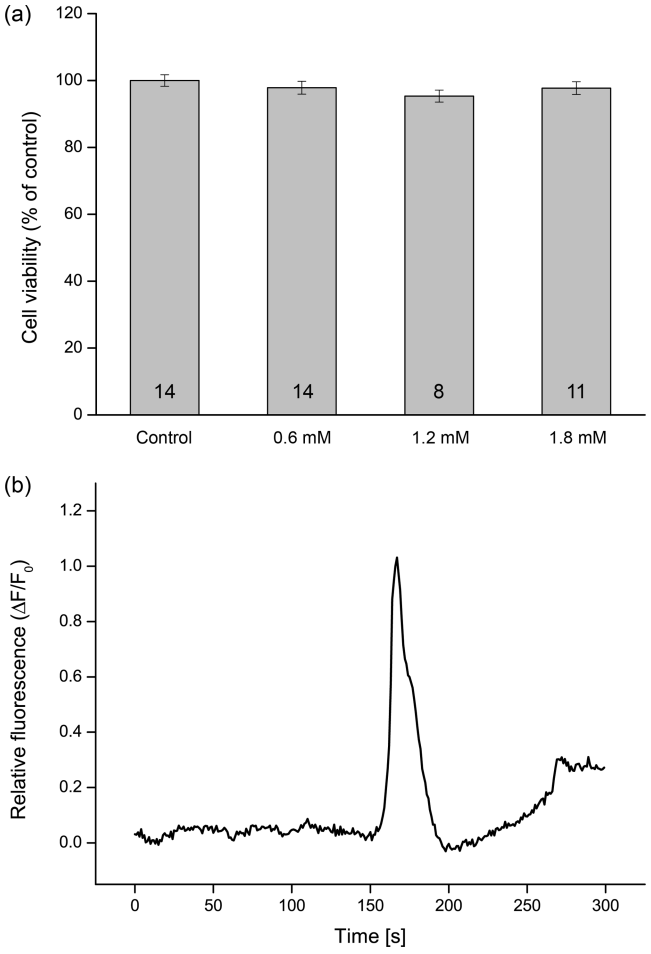

Figure 6. Cell viability and responsiveness are not compromised by SCA. (a) Cell viability assays (MTT) performed 4 h after acute exposure to different concentrations of SCA (0.6, 1.2, and 1.8 mM). Number of assays performed are presented at bases of the bars. (b) Astrocytes responded to 1 mM ATP in the presence of 1.2 mM SCA, 45 min after exposure to the probe. The graph depicts an average calcium transient ($n = 11$) in response to 1 mM ATP.

SCA concentration is still available for interaction with Ca^{2+}, since SCA and Ca^{2+} interact in the extracellular volume, while only water distributes throughout the intra- and extracellular volume.

From the simulations, we found that the greatest Ca^{2+}-induced change in T_1 was slightly above 7% (Table 2). However, this change can only occur in the absence of cells, provided that the concentrations of the SCA and Ca^{2+} are similar, or that the SCA has a greater concentration than Ca^{2+}. At SCA concentrations half those of Ca^{2+}, activation induces much lower T_1 changes (~2%). In the presence of cells (conditions equivalent to the in vitro experiments in Matrigel), the maximal changes were only slightly reduced in comparison to experiments in CCM alone. Likewise, in vivo, owing to its low extracellular fraction and higher baseline T_1, the Ca^{2+}-induced changes were up to 6%, again at $[SCA] \geq [Ca^{2+}]$.

DISCUSSION

The relaxometric titrations of GdL with Ca^{2+} exhibited a drop in r_1 for samples with higher Ca^{2+} concentrations, measured >2 h after the solutions were prepared (see above). This effect was probably caused by changes in bicarbonate/carbonate ratios

dx.doi.org/10.1021/cn500049n | ACS Chem. Neurosci. 2014, 5, 360−369

Table 2. Prediction of T_1 Relaxation Times Expected for Gd_2L at Two Ca^{2+} Concentrations, Absolute T_1 Difference, and Percent Change in T_1 for Three Conditions[a]

	baseline T_1 $[Ca^{2+}]$ = 1.2 mM	activation T_1 $[Ca^{2+}]$ = 0.8 mM	ΔT_1	change from the baseline T_1
[SCA] in CCM				
0.6 mM	214.7 ms	218.4 ms	3.7 ms	1.7%
1.2 mM	117.3 ms	126.3 ms	9.0 ms	7.7%
1.8 mM	85.4 ms	92.1 ms	6.7 ms	7.8%
[SCA] in cellular model				
0.6 mM	309.2 ms	314.2 ms	5.0 ms	1.6%
1.2 mM	174.0 ms	186.8 ms	12.8 ms	7.4%
1.8 mM	128.0 ms	137.7 ms	9.7 ms	7.6%
[SCA] in vivo				
0.6 mM	654.4 ms	661.3 ms	6.9 ms	1.1%
1.2 mM	434.5 ms	458.6 ms	24.1 ms	5.6%
1.8 mM	340.4 ms	361.3 ms	20.8 ms	6.1%

[a]Three conditions: in CCM only (estimated extracellular fraction, EF = 1), the cellular model presented in this work (EF = 0.65), and in vivo (EF = 0.20). For each condition, three different SCA concentrations are considered.

over time in the solution. The increased influence of carbonates on the Gd-DO3A moiety then led to ternary complex formation, reduction of hydration number, and consequently lower r_1.[15] However, this phenomenon would not be expected to take place in vivo where the bicarbonate concentration and the pH are efficiently buffered.

Additionally, a number of important findings were revealed with the experiments described above. First, despite the high complexity of the 3D cell culture perfusion model used here, the results indicated the following: (a) there was "an active volume effect" for our SCA, because the partial ECS volume results in lower MR signal changes detected from the SCA; (b) the small but significant MR signal changes induced by SCA are reversible, thus potentially allowing long-term studies of neuronal activity rather than a "one-shot" study. The slightly elevated T_1 values when comparing the recovered with initial "resting state" conditions suggest that the total duration of the experiment and drastic perturbations in Ca^{2+} concentration affect cell physiology in our model system, and lead to the unreliability of values obtained more than 3−4 h after beginning the experiment. However, we have also observed that the duration of the experiment solely depends on local physiological conditions, while SCA integrity and activity remains intact during the course of the whole experiment.

Second, the fluorescence imaging study on astrocytes in culture demonstrated that, by lowering the concentration of cytosolic Ca^{2+} to a new stable level, SCA probably changes the concentration gradient of this ion at the plasma membrane. Intracellular calcium redistribution is accomplished mostly through SOCE channels in the plasma membrane, although SERCA and NCX pathways also have a significant role. Interestingly, the decreased level of cytosolic Ca^{2+} remains the same regardless of the SCA concentration. This may indicate that upon being perturbed by SCA the above transport mechanisms function in synergy in order to keep a different but stable Ca^{2+} homeostatic state. Nevertheless, the cells remain functional and responsive to stimulation by ATP.

Third, the relaxation time estimates at rested and activated states yield T_1 values that significantly differ from each other. It is to note that actual SCA concentration plays a critical role for the level of the expected changes. The estimates suggest higher response to Ca^{2+} when SCA concentration is equimolar or higher than its target ($[SCA] \geq [Ca^{2+}]_o$, Table 2). Therefore, a good control over the local [SCA] and concomitantly $[Gd^{3+}]$ is necessary in order to assign the signal changes to variations in the target concentration (Ca^{2+}) rather than, for example, changes of the SCA concentration due to the diffusion. Various approaches to circumvent this problem have been developed recently for pH-sensitive MRI agents and could in principle be used for SCAs in general.[32−34]

The estimates also show that the level of T_1 changes advantageously does not drop proportional to the EF decrease, even though the extracellular fraction (EF) decreases and a lower SCA concentration is expected in vivo than in our in vitro experiments. Nevertheless, the predicted values were 2−3 times larger than actually observed in the cell experiments, stressing the great complexity of in vitro/in vivo experiments and apparent difficulty to experimentally achieve theoretically expected values.

Overall, the results obtained in the experimental and modeling studies described above are positive and encourage further development of this potenitally novel fMRI methodology. Although the partial extracellular volume is much lower than the intracellular one, targeting extracellular Ca^{2+} is very reasonable. Its local concentrations outside are much higher than those inside the cell; hence, the robust changes in the level of 0.3−0.4 mM are very favorable for less sensitive methods like MRI, where concentrations of the SCA and its target at the same order of magnitude are required ($[SCA] \geq [Ca^{2+}]_o$). On the other hand, such high levels of SCA would be probably impossible to achieve in vivo by an intravenous SCA administration; therefore, more invasive intraventricular or intracerebral injections may ensure appropriate local SCA concentration.[29,35]

The fluorescence microscopy experiments revealed that SCA affects the intracellular Ca^{2+} level by lowering it. Nevertheless, SCA is not toxic to the cells, while, very importantly, Ca^{2+} transport through the plasma membrane is unaffected by the agent. Intracellular Ca^{2+}-signaling (triggered in our case by stimulation with ATP) occurs despite the presence of relatively high SCA concentrations (max. 1.8 mM), demonstrating normal cellular functions under such conditions.

Finally, despite a strong attenuation of the MRI signal due to the lower EF, estimated T_1 changes caused by SCA document the feasibility of monitoring extracellular Ca^{2+} changes by means of MRI. Principally, these changes could be followed in a dynamic manner, to allow tracking neuronal activity with high temporal (subsecond) resolution, certainly better than the current BOLD-based fMRI (2−3 s).[6,36] Along these lines, execution of T_1-weighted MRI experiments would be preferable to attain high temporal resolution (opposite to T_1-mapping as directly comparable to results presented here). Considering the obtained T_1 estimates (Table 2), the desired MRI experiment with high temporal resolution (T_1-weighted experiments) may result in signal changes with the same or lower level than those obtained in temporaly slower T_1-mapping MRI experiments.

We also note that our estimates considered only T_1 changes directly caused by SCA, thus excluding many aspects and obstacles relevant for in vivo experiments, such as other sources of T_1 signals (e.g., iron in the blood), blood inflow effects, or SCA diffusion. Moreover, the results and potential signal changes depend on additional parameters such as the imaging hardware and protocols (the applied sequence, imaging

dx.doi.org/10.1021/cn500049n | ACS Chem. Neurosci. 2014, 5, 360−369

parameters, T_E, T_R, etc.). Given that the level of signal changes produced by SCA in this work are comparable to BOLD-based fMRI,[37] it will be certainly necessary to develop specific experimental and data analysis protocols that ensure the appropriate statistical significance to support any of conclusions obtained in the experiments employing this methodology.

CONCLUSIONS

This work is a continuation of attempts to validate the feasibility of SCA for tracking biological processes in vivo.[36,38] Here, we go beyond theoretical simulations and report in vitro experiments supporting the theoretical data and confirming potential practical utilization. The experimental methodologies used suggest that SCA produces signal changes that may be detectable by the appropriate instrumentation, and that SCA administration does not affect the regular cellular physiology to any great extent. Currently, the delivery of relatively high levels of SCA and the possibility of observing such weak MRI signal changes remain the major limitations of this methodology which need to be improved in the future. Nevertheless, further advances can contribute enormously to the ultimate practical establishement of this methodology. In this work, we discussed only the potential T_1 and MR signal changes in vivo originated by the specific SCA developed by us. Nevertheless, the continuous chemistry efforts are expected to further improve the SCA activity, resulting in SCA with even stronger alterations in r_1, and subsequently higher MR signal changes. Furthermore, progress in MRI hardware or methodology by MRI engineers and physicists, such as development of dedicated sequences for fast imaging that exclude parallel MRI signals and extract only the relevant ones, would enable validation of this approach and the establishment of the crucial role of chemistry in this complex but potentially extremely beneficial research. The development of such fMRI methodology able to follow neuronal activity noninvasively in manner superior to BOLD would be a great asset in neuroimaging and molecular imaging techniques, leading us to much better understanding of essential physiological processes in living organisms.

METHODS

General Remarks. Gd_2L was synthesized according to the modified procedure published recently by our group.[39] $^{31}P\{^1H\}$ NMR spectra were recorded on a Bruker Avance III 300 MHz (7.0 T) spectrometer at 37 °C. The ^1H T_1 determinations were performed with the same instrument at 37 °C, using a standard inversion recovery pulse sequence. Matrigel Basement Membrane Matrix was purchased from BD Biosciences, Germany, while the Polybead microspheres were purchased from Polysciences Europe GmbH, Germany. Cell culture medium (CCM) was prepared from Ca^{2+}-free Dulbecco's modified Eagle's medium (DMEM, Biochrom AG, Germany) supplemented with 10% fetal bovine serum, 4 mM L-glutamine, 100 μg/mL streptomycin, and 100 U/mL penicillin (all from Biochrom AG, Germany). The external solution for the astrocyte cell cultures consisted of NaCl (130 mM), KCl (5 mM), $CaCl_2$ (2 mM), $MgCl_2$, (1 mM), D-glucose (10 mM), and HEPES (10 mM, pH 7.4, adjusted with NaOH). For the Ca^{2+}-free external solution, $CaCl_2$ was omitted and Na_4EGTA (0.1 mM) was added.

Relaxometric Titrations. Experiments were performed in two different ways. Method A: a solution of $CaCl_2$ of known concentration was added stepwise to a solution of SCA (starting concentration 1.8 mM Gd_2L = 3.6 mM Gd^{3+}), and the longitudinal proton relaxation time T_1 was measured after each addition of the analyte. Method B: separate SCA solutions were prepared (1.0 mM Gd_2L = 2.0 mM Gd^{3+}), with each solution containing different Ca^{2+} concentration. T_1 was measured for each solution separately. For both methods, the r_1 was calculated from eq 1 using the actual Gd^{3+} concentration at each point of the titration. $T_{1,obs}$ is the observed longitudinal relaxation time, $T_{1,d}$ is the diamagnetic contribution in the absence of the paramagnetic substance, and [Gd] is the concentration of Gd^{3+}. The initial Gd^{3+} concentrations were determined by measuring the bulk magnetic susceptibility shifts.[40]

$$\frac{1}{T_{1,\mathrm{obs}}} = \frac{1}{T_{1,\mathrm{d}}} + r_1 \times [\mathrm{Gd}] \quad (1)$$

NMR Studies of SCA with Cells in a 3D Cell Culture Model. The 3D cell culture perfusion system described by Brand et al.[18] and Flögel et al.[41] was adapted to 5 mm NMR tubes. In brief, NIH-3T3 embryonic mouse fibroblast cells (DSMZ, Germany) were grown as monolayers in Ca^{2+}-containing CCM (Ca-CCM) to confluence. Cells were then harvested by trypsinization and embedded in Matrigel threads.[17] For this, ~0.5×10^6 cells were mixed with ice-cold Matrigel (1:1, v/v) and kept on ice. The cold mixture was drawn into sterile Teflon tubing attached to a syringe filled with medium. Immersing the tubing in 37 °C warm water gelled the mixture in 2 min, and afterward the threads were extruded into non-tissue-culture-treated Petri dishes filled with Ca-CCM. After 3−4 days, the threads were almost completely filled with cells and ~10^7 cells were used for the NMR studies. Threads were transferred into a 5 mm NMR tube which was sealed with the perfusion insert (Figure 2). Differing from analogous setups mentioned above,[18,41] a second peristaltic pump (both Heidolph, Germany) was used as a backup pump. Namely, due to the small diameter of the NMR tube used here (5 mm instead of 10 mm) and consequently the smaller inner diameters of the tubing (510 μm), it was necessary to use this second pump to prevent overflow of circulating medium out of the NMR tube. For the same reasons, porous disk frits with a pore size of 70 μm (cut from Thomapor, Reichelt Chemietechnik GmbH & Co., Germany) were used. Once inside the closed perfusion system, the embedded cells were perfused with CCM thermostated at 37 °C, supplemented with the required Ca^{2+} concentration and 20 mM HEPES for pH-buffering. Also, the CCM was constantly oxygenated with Carbogen gas (95% O_2/5% CO_2) directly bubbled into the medium. The flow rate of the medium was adjusted to ~500 μL/min. During the inversion recovery experiment acquisition (~5 min), the perfusion was stopped. For re-equilibrium, the flow rate was increased stepwise over 1 min to the initial flow rate of 500 μL/min to prevent pressure build-up. The cells were perfused for at least another 4 min before the next acquisition was done. At each condition, T_1 was determined in triplicate by three consecutive measurements. Mean ± SEM was calculated for each of the conditions in a single experiment. The mean ΔT_1 of "activated state" vs initial "resting state" was determined and averaged over all three experiments.

If not otherwise stated, values represent mean ± SEM. Statistical analyses were performed by ANOVA (applying Tukey's multiple comparison post-test) or unpaired Student's *t*-test using Graphpad Prism 5.03.

Astrocyte Cell Cultures. Primary cortical astrocyte cultures were prepared from the cerebral cortices of neonatal P2 rats as described previously.[42] The experimental animals were cared for in accordance with the European Convention for the Protection of Vertebrate Animals used for Experimental and other Scientific purposes (Council of Europe No. 123, Strasbourg, 1985), and approved by the Ethical Committee of the Faculty of Biology, University of Belgrade. Briefly, after brain dissection, the cortices were isolated and mechanically dissociated under sterile conditions in isolation medium (Leibovitz L-15 medium supplemented with 2 mM L-glutamine, 100 U/mL penicillin, 0.1 mg/mL streptomycin, and 0.1% bovine serum albumin). After two centrifugation washing steps (500*g*, 4 min), the cell suspension was passed through 21 and 23 G sterile needles (to remove the residual tissue aggregates) followed by a final centrifugation washing step (500*g*, 4 min). Cells were then resuspended in growth medium (DMEM) with 4.5 g/L glucose, supplemented with 10% fetal bovine serum, 2 mM L-glutamine, 1 mM sodium-pyruvate, 100 U/mL

dx.doi.org/10.1021/cn500049n | ACS Chem. Neurosci. 2014, 5, 360−369

penicillin, and 0.1 mg/mL streptomycin), plated on cell-culture flasks (one cortex per 75 cm^2), and grown in a humidified atmosphere of 5% CO_2/95% air at 37 °C. Cells were fed every third day until reaching confluence (9 days) before being shaken at 350 rpm for 20 h on a plate shaker (PerkinElmer, Turku, Finland) to remove any remaining oligodendrocytes and microglia. Cells were then replated (1:4) on cell culture flasks (25 cm^2) for further use. After reaching confluence again, cells were subcultured onto 25 mm diameter poly-L-lysine-coated coverslips (1.5×10^5 cells/cm^2) and used within 2−4 days. The purity of astroglial culture (~95%) was assessed by immunocytochemical detection of the glial fibrillary acidic protein.

Pharmacological Agents. Astrocytes were incubated with specific blockers of intracellular calcium pumps and plasma membrane channels and exchangers, for 5−10 min at room temperature in the external solution: (1) 100 μM benzamil hydrochloride (Sigma-Aldrich, Deisenhofen, Germany), potent blocker of plasma membrane sodium−calcium exchanger (NCX); (2) 1 μM thapsigargin (Tocris Bioscience, U.K.), an effective inhibitor of sarco-endoplasmatic reticulum Ca^{2+}-ATPases (SERCA); (3) combination of 10 μM $LaCl_3$, 10 μM $GdCl_3$ (both from Sigma-Aldrich, Deisenhofen, Germany), and 75 μM 2-aminoethoxydiphenyl borate (2-APB, Tocris Biocsience, U.K.), which in higher concentrations readily blocks the SOCE channels. Thereafter, astrocytes were treated with SCA, as described above.

Intracellular Calcium Imaging and Data Analysis. Intracellular calcium concentrations in astrocytes were assessed using the cell-permeable acetoxymethyl (AM) ester of Fluo-4 (Fluo-4 AM, Molecular Probes). Astrocytes were loaded with 5 μM Fluo-4 AM for 30 min in external solution at room temperature. After 3 washes, before imaging, cells were kept in working solution (external solution with/without Ca^{2+}) for an additional 15−20 min at room temperature to allow de-esterification of the dye. In a subset of experiments, astrocytes were incubated with the pharmacological agents as described above. Cell-loaded coverslips were transferred into the recording chamber on a confocal microscope (LSM510, Zeiss, Jena, Germany) equipped with water immersion objective 40× (NA 0.8) and supplied with 800 μL of working solution (external solution with/without Ca^{2+} and/or pharmacological agents). Fluo-calcium indicator was excited with an argon ion laser (488 nm), and the emission light filtered with a long-pass 505 nm filter. Time-lapse images were obtained every 3 s for 15−45 min. Initially, fluorescence intensities were recorded for 2−5 min to determine the baseline fluorescence (F_0). Thereafter, astrocytes were treated with three concentrations of SCA (0.6, 1.2, and 1.8 mM) by bolus addition of 50−175 μL of a 10 mM SCA solution. Fluorescence data were expressed as $\Delta F/F_0$ (%), where ΔF represents the change in fluorescence emission.

Cell Viability Assay. Cell viability was determined by evaluating total mitochondrial activity using the MTT (3-[4,5-dimethylthiazol-2-yl]-2,5-diphenyl tetrazolium bromide) assay (Sigma-Aldrich, St. Louis, MO). Astrocytes were seeded into 96-well plates (15×10^3 cells/well) in growth medium. After 2 days, cells were treated with SCA (0.6, 1.2, and 1.8 mM) in growth medium for 4 h. Subsequently, new growth medium containing 0.5 mg/mL MTT was added to the cells, and cells were kept for another 2.5 h at 37 °C. After removing the medium, formazan generated by total mitochondrial activity was dissolved in DMSO and optical density was measured at 540 nm with an LKB 5060 multiplate reader. Measurements were performed in sextuplicates, and the viability of treated cells was expressed as percentage of untreated controls.

Curve Fitting of Relaxometric Experiments and T_1 Estimations. The experimental data from each of seven independent experiments performed in CCM were fitted to eq 2, a slightly modified dissociation equation reported elsewhere,[35] since the bismacrocycles carry two Gd^{3+} per SCA (therefore the term [Gd] was in this case replaced by [SCA]). The equation assumed a single binding site (n = 1), while the $r_{1,obs}$ is the observed relaxivity, $r_{1,f}$ and $r_{1,b}$ are relaxivities of free and fully bound SCA, respectively, $[Ca^{2+}]$ and [SCA] are concentrations of Ca^{2+} and SCA, respectively, K_d is the equilibrium dissociation constant, and $A = [SCA] + [Ca^{2+}] + K_d$. Finally, mean ± SD were calculated for the three fitted parameters K_d, $r_{1,f}$, and $r_{1,b}$.

$$r_{1,obs} = r_{1,f} \times [SCA] + (r_{1,b} - r_{1,f}) \times \frac{A - \sqrt{A^2 - 4 \times [SCA] \times [Ca^{2+}]}}{2 \times [SCA]} \quad (2)$$

For the in vitro conditions without cells, we assumed that the relaxation time $T_{1,d}$ in the absence of the contrast agent is 2.85 s. In the presence of cells, the $T_{1,d}$ was set to 2.3 s (unpublished data, measured in a different series of eight experiments in cell pellets at 7 T, with an extracellular fraction (EF) of 0.5−0.65). The EF was set to 0.65 for the prediction of T_1 in our presented 3D cellular model (Table 2). For the in vivo condition, we assumed that $T_{1,d}$ = 1.5 s, which is expected at 7 T[43] and that EF = 0.20.[16] The exact r_1 relaxivity values for each state (activation, baseline) were obtained from the curve fits. The estimated T_1 ($T_{1,est}$) was then calculated while accounting for the effective gadolinium concentration (1.2, 2.4, or 3.6 mM, [Gd] = 2[SCA]), and the extracellular fraction according to eq 3 where $T_{1,d}$ is the diamagnetic contribution at different EF, r_1 is the relaxivity value obtained from the curve fits, and [Gd] is the actual Gd^{3+} concentration at each point of the titration.

$$\frac{1}{T_{1,est}} = \frac{1}{T_{1,d}} + r_1 \times [Gd] \times EF \quad (3)$$

AUTHOR INFORMATION

Corresponding Author

*E-mail: goran.angelovski@tuebingen.mpg.de. Tel: +49 7071 601 916. Fax: +49 7071 601 919.

Author Contributions

G.A. designed research; P.K. prepared the studied contrast agent; G.A. and S.G. performed NMR experiments with cells and analyzed data together with J.E.; M.M. and P.A. performed astrocyte studies and analyzed results; G.E.H. performed fitting and estimations of T_1 values; N.K.L. supported research; all authors wrote the manuscript.

Funding

This work was supported from the Max-Planck Society, German Research Foundation (DFG, Grant AN 716/2-1), German Ministry for Education and Research (BMBF, FKZ: 01EZ0813), MESTD RS (Grant No. 41005), and a grant from the Ministry of Science, Research and the Arts of Baden-Wuerttemberg (AZ: 32-771-8-1504.12/1/1) to GEH.

Notes

The authors declare no competing financial interest.

ACKNOWLEDGMENTS

This work was performed within the frame of European COST D38, CM1006, and TD1004 Actions. The authors thank Martin Voetsch and Andrej Korenić for help in preparing graphics.

REFERENCES

(1) Hofer, A. M. (2005) Another dimension to calcium signaling: a look at extracellular calcium. *J. Cell Sci. 118*, 855−862.

(2) Grynkiewicz, G., Poenie, M., and Tsien, R. Y. (1985) A New Generation of Ca^{2+} Indicators with Greatly Improved Fluorescence Properties. *J. Biol. Chem. 260*, 3440−3450.

(3) Looger, L. L., and Griesbeck, O. (2012) Genetically encoded neural activity indicators. *Curr. Opin. Neurobiol. 22*, 18−23.

(4) Smith, G. A., Hesketh, R. T., Metcalfe, J. C., Feeney, J., and Morris, P. G. (1983) Intracellular Calcium Measurements by ^{19}F NMR of Fluorine-Labeled Chelators. *Proc. Natl. Acad. Sci. U.S.A. 80*, 7178−7182.

(5) Ogawa, S., Lee, T. M., Nayak, A. S., and Glynn, P. (1990) Oxygenation-Sensitive Contrast in Magnetic-Resonance Image of Rodent Brain at High Magnetic-Fields. *Magn. Reson. Med. 14*, 68−78.
(6) Logothetis, N. K. (2008) What we can do and what we cannot do with fMRI. *Nature 453*, 869−878.
(7) Li, W. H., Fraser, S. E., and Meade, T. J. (1999) A calcium-sensitive magnetic resonance imaging contrast agent. *J. Am. Chem. Soc. 121*, 1413−1414.
(8) Angelovski, G., and Mamedov, I. (2011) Cation-Responsive MRI Contrast Agents Based on Gadolinium(III). *Curr. Inorg. Chem. 1*, 76−90.
(9) Atanasijevic, T., Shusteff, M., Fam, P., and Jasanoff, A. (2006) Calcium-sensitive MRI contrast agents based on superparamagnetic iron oxide nanoparticles and calmodulin. *Proc. Natl. Acad. Sci. U.S.A. 103*, 14707−14712.
(10) Angelovski, G., Chauvin, T., Pohmann, R., Logothetis, N. K., and Tóth, É. (2011) Calcium-Responsive Paramagnetic CEST Agents. *Bioorg. Med. Chem. 19*, 1097−1105.
(11) Somjen, G. G. (2004) *Ions in the brain: normal function, seizures, and strokes*, Oxford University Press, New York; Oxford.
(12) Nicholson, C., ten Bruggencate, G., Steinberg, R., and Stöckle, H. (1977) Calcium modulation in brain extracellular microenvironment demonstrated with ion-selective micropipette. *Proc. Natl. Acad. Sci. U.S.A. 74*, 1287−1290.
(13) Nicholson, C., ten Bruggencate, G., Stockle, H., and Steinberg, R. (1978) Calcium and potassium changes in extracellular microenvironment of cat cerebellar cortex. *J. Neurophysiol. 41*, 1026−1039.
(14) Angelovski, G., Fouskova, P., Mamedov, I., Canals, S., Toth, E., and Logothetis, N. K. (2008) Smart magnetic resonance imaging agents that sense extracellular calcium fluctuations. *ChemBioChem 9*, 1729−1734.
(15) Botta, M., Aime, S., Barge, A., Bobba, G., Dickins, R. S., Parker, D., and Terreno, E. (2003) Ternary complexes between cationic Gd-III chelates and anionic metabolites in aqueous solution: An NMR relaxometric study. *Chem.—Eur. J. 9*, 2102−2109.
(16) Nicholson, C., and Sykova, E. (1998) Extracellular space structure revealed by diffusion analysis. *Trends Neurosci. 21*, 207−215.
(17) Daly, P. F., Lyon, R. C., Straka, E. J., and Cohen, J. S. (1988) ^{31}P-NMR Spectroscopy of Human Cancer-Cells Proliferating in a Basement-Membrane Gel. *FASEB J. 2*, 2596−2604.
(18) Brand, A., Richter-Landsberg, C., Flögel, U., Willker, W., and Leibfritz, D. (1998) Rat brain primary neurons immobilized in basement membrane gel threads: An improved method for on-line ^{13}C NMR spectroscopy of live cells. *Brain. Res. Protoc. 3*, 183−191.
(19) Verkhratsky, A., Orkand, R. K., and Kettenmann, H. (1998) Glial calcium: Homeostasis and signaling function. *Physiol. Rev. 78*, 99−141.
(20) Haydon, P. G., and Parpura, V. (2009) *Astrocytes in (Patho) Physiology of the Nervous System*, Springer, New York.
(21) Parpura, V., Grubisic, V., and Verkhratsky, A. (2011) Ca^{2+} sources for the exocytotic release of glutamate from astrocytes. *Biochim. Biophys. Acta, Mol. Cell Res. 1813*, 984−991.
(22) Vaca, L. (2010) SOCIC: The store-operated calcium influx complex. *Cell Calcium 47*, 199−209.
(23) Verkhratsky, A., Rodriguez, J. J., and Parpura, V. (2012) Calcium signalling in astroglia. *Mol. Cell. Endocrinol. 353*, 45−56.
(24) Hoth, M., and Penner, R. (1993) Calcium Release-Activated Calcium Current in Rat Mast-Cells. *J. Physiol. 465*, 359−386.
(25) Parekh, A. B., and Putney, J. W. (2005) Store-operated calcium channels. *Physiol. Rev. 85*, 757−810.
(26) Treiman, M., Caspersen, C., and Christensen, S. B. (1998) A tool coming of age: thapsigargin as an inhibitor of sarcoendoplasmic reticulum Ca^{2+}-ATPases. *Trends Pharmacol. Sci. 19*, 131−135.
(27) Fischer, K. G., Jonas, N., Poschenrieder, F., Cohen, C., Kretzler, M., Greiber, S., and Pavenstadt, H. (2002) Characterization of a Na^+-Ca^{2+} exchanger in podocytes. *Nephrol., Dial., Transplant. 17*, 1742−1750.
(28) Benz, B., Grima, G., and Do, K. Q. (2004) Glutamate-induced homocysteic acid release from astrocytes: Possible implication in glia-neuron signaling. *Neuroscience 124*, 377−386.
(29) Mamedov, I., Canals, S., Henig, J., Beyerlein, M., Murayama, Y., Mayer, H. A., Logothetis, N. K., and Angelovski, G. (2010) In Vivo Characterization of a Smart MRI Agent That Displays an Inverse Response to Calcium Concentration. *ACS Chem. Neurosci. 1*, 819−828.
(30) Nobile, M., Monaldi, I., Alloisio, S., Cugnoli, C., and Ferroni, S. (2003) ATP-induced, sustained calcium signalling in cultured rat cortical astrocytes: evidence for a non-capacitative, P2 × 7-like-mediated calcium entry. *FEBS Lett. 538*, 71−76.
(31) Zorec, R., Araque, A., Carmignoto, G., Haydon, P. G., Verkhratsky, A., and Parpura, V. (2012) Astroglial excitability and gliotransmission: an appraisal of Ca^{2+} as a signalling route. *ASN Neuro 4*, 103−119.
(32) Gianolio, E., Napolitano, R., Fedeli, F., Arena, F., and Aime, S. (2009) Poly-beta-cyclodextrin based platform for pH mapping via a ratiometric ^{19}F/^{1}H MRI method. *Chem. Commun.*, 6044−6046.
(33) Frullano, L., Catana, C., Benner, T., Sherry, A. D., and Caravan, P. (2010) Bimodal MR-PET Agent for Quantitative pH Imaging. *Angew. Chem., Int. Ed. 49*, 2382−2384.
(34) Gianolio, E., Maciocco, L., Imperio, D., Giovenzana, G. B., Simonelli, F., Abbas, K., Bisi, G., and Aime, S. (2011) Dual MRI-SPECT agent for pH-mapping. *Chem. Commun. 47*, 1539−1541.
(35) Hagberg, G. E., Mamedov, I., Power, A., Beyerlein, M., Merkle, H., Kiselev, V. G., Dhingra, K., Kubìček, V., Angelovski, G., and Logothetis, N. K. (2014) Diffusion properties of conventional and calcium-sensitive MRI contrast agents in the rat cerebral cortex. *Contrast Media Mol. Imaging 9*, 71−82.
(36) Shapiro, M. G., Atanasijevic, T., Faas, H., Westmeyer, G. G., and Jasanoff, A. (2006) Dynamic imaging with MRI contrast agents: quantitative considerations. *Magn. Reson. Imaging 24*, 449−462.
(37) Jasanoff, A. (2007) Bloodless fMRI. *Trends Neurosci. 30*, 603−610.
(38) Ahrens, E. T., Rothbacher, U., Jacobs, R. E., and Fraser, S. E. (1998) A model for MRI contrast enhancement using T_1 agents. *Proc. Natl. Acad. Sci. U.S.A. 95*, 8443−8448.
(39) Kadjane, P., Logothetis, N. K., and Angelovski, G. (2011) A straightforward and convenient pathway for the synthesis of functional bismacrocyclic ligands. *Tetrahedron Lett. 52*, 1619−1622.
(40) Corsi, D. M., Platas-Iglesias, C., van Bekkum, H., and Peters, J. A. (2001) Determination of paramagnetic lanthanide(III) concentrations from bulk magnetic susceptibility shifts in NMR spectra. *Magn. Reson. Chem. 39*, 723−726.
(41) Flögel, U., Willker, W., and Leibfritz, D. (1994) Regulation of Intracellular pH in Neuronal and Glial Tumor-Cells, Studied by Multinuclear NMR Spectroscopy. *NMR Biomed. 7*, 157−166.
(42) McCarthy, K. D., and de Vellis, J. (1980) Preparation of Separate Astroglial and Oligodendroglial Cell-Cultures from Rat Cerebral Tissue. *J. Cell. Biol. 85*, 890−902.
(43) Rooney, W. D., Johnson, G., Li, X., Cohen, E. R., Kim, S.-G., Ugurbil, K., and Springer, C. S., Jr. (2007) Magnetic Field and Tissue Dependencies of Human Brain Longitudinal ^1H_2O Relaxation in Vivo. *Magn. Reson. Med. 57*, 308−318.